



DOI: 10.29026/oea.2020.200023

Helicity-dependent THz emission induced by ultrafast spin photocurrent in nodal-line semimetal candidate Mg_3Bi_2

Mingyu Tong^{1†}, Yuze Hu^{1†}, Xiangnan Xie³, Xiegang Zhu⁵,
Zhenyu Wang^{2,4*}, Xiang'ai Cheng¹ and Tian Jiang^{1*}

Helicity-dependent ultrafast spin current generated by circularly polarized photons in topological materials holds the crux to many technological improvements, such as quantum communications, on-chip communication processing and storage. Here, we present the manipulation of helicity-dependent terahertz emission generated in a nodal line semimetal candidate Mg_3Bi_2 by using photon polarization states. The terahertz emission is mainly ascribed to the helicity-dependent photocurrent that is originated from circular photogalvanic effects, and the helicity-independent photocurrent that is attributed to linear photogalvanic effect. Our work will inspire more explorations into novel nodal line semimetals and open up new opportunities for developing ultrafast optoelectronics in the topological system.

Keywords: terahertz; spin photocurrent; nodal-line semimetal; topological material

Tong M Y, Hu Y Z, Xie X N, Zhu X G, Wang Z Y et al. Helicity-dependent THz emission induced by ultrafast spin photocurrent in nodal-line semimetal candidate Mg_3Bi_2 . *Opto-Electron Adv* 3, 200023 (2020).

Introduction

Generation and control of an ultrafast spin-photocurrent in topological materials are of great significance¹. On the one hand, the spin-photocurrent generated in a picosecond timescale permits ultrafast optical manipulation². Proverbially, efficient devices could be realized for data storage and processing if the spin degree of freedom is utilized³. However, the processing of information calls for the generation and control of spin current in transient time to achieve ultrafast operations, especially at frequencies coming up to the undeveloped terahertz band⁴. Fortunately, the unique chiral behavior of spin photocurrent in topological materials permits the ultrafast operation under circularly polarized light

without an external bias field⁵. On the other hand, the spin-photocurrent induced electromagnetic wave in the terahertz frequency domain has been proven to be an efficient helical terahertz (THz) emitter^{6,7}. It is worth mentioning that the generation and manipulation of helical THz pulses in the past mainly depend on the complicated pulse shaping or two color manipulation of the incident laser while emitters possess no intrinsic optical chirality⁸. Therefore, the ability to explore the topological materials with peculiar spin-momentum locking or chiral properties is of crucial importance.

Nodal-line semimetals (NLSs), which host one-dimensional closed-loop or line degeneracies formed by the crossing of two bands, have been proposed recently as a family of topological phase materials^{9–11}. The

¹College of Advanced Interdisciplinary Studies, National University of Defense Technology, Changsha 410073, China. ²National Innovation Institute of Defense Technology, Academy of Military Sciences PLA China, Beijing 100010, China. ³State Key Laboratory of High Performance Computing, College of Computer, National University of Defense Technology, Changsha 410073, China. ⁴Beijing Academy of Quantum Information Sciences, Beijing 100193, China. ⁵Science and Technology on Surface Physics and Chemistry Laboratory, Jianguyou 621908, China.

[†]These authors contributed equally to this work.

*Correspondence: Z Y Wang, E-mail: oscarwang2008@sina.com; T Jiang, E-mail: tjiang@nudt.edu.cn

Received: 24 June 2020; Accepted: 15 September 2020; Published: 24 December 2020

distinguishing characteristic of NLSs is their two dimensional (2D) drumhead-like surface states, which are embedded into the ‘direct gap’ between conduction and valence band in the 2D projection of the nodal ring^{9,12–14}. Up to now, NLSs have been intensively studied in many compounds such as PtSn₄¹⁵, Cu₃PdN¹⁴, PbTaSe₂¹¹, TlTaSe₂¹², Mg₃Bi₂¹⁶. Among them, Mg₃Bi₂ is a significant thermoelectric material with excellent performance in the process of energy conversion¹⁷. The good thermoelectric performance of Mg₃Bi₂-based materials may be closely related to its topological properties²⁰. Mg₃Bi₂ is predicted to be NLSs in the absence of spin-orbit coupling (SOC) and become a strong topological insulator when SOC is considered¹⁶. Taking SOC into consideration in the calculation, the drumhead surface band would split and transform into topological surface states, with a small bulk energy gap of about 35 meV opening at the line nodes¹⁶. However, the topological properties can hardly be enclosed by experiments due to the heavily p-doped Mg vacancies^{16,18}. Thus, Mg₃Bi₂ is usually called as a candidate for NLSs. Fortunately, a recent work has revealed that Mg₃Bi₂ is a semimetal with topological surface states by in-situ angle resolved photoemission spectroscopy (ARPES)¹⁸, and further investigation for the optical properties of Mg₃Bi₂ is still in need.

In this paper, we exploit the chiral-controlled spin photocurrent in nodal line semimetal candidate Mg₃Bi₂ through terahertz emission spectroscopy. By investigating the emitted THz electromagnetic wave

under the photon injection, we found the polarity and chirality of the photocurrents can be manipulated by polarized near-infrared optical pump on a picosecond timescale. In addition, we demonstrate that the chirality-dependent terahertz emission is mainly originated from the circular photogalvanic effect (CPGE), which is associated with the angular momentum selection rules of topological surface states.

Results and discussion

Materials growth and characterization

Mg₃Bi₂ is a layered Kagome lattice structure with the space group of $P\bar{3}m1$, as shown in Figs. 1(a) and 1(b). Mg and Bi atoms assemble in layers naturally with five atomic layers stacking along the (001) crystal orientation¹⁸. Mg₃Bi₂ thin films were grown on the transparent sapphire (Al₂O₃) substrates by using molecular beam epitaxy. A Se capping layer is essential to protect the Mg₃Bi₂ film from oxidation in the atmosphere and prevent the thin film from the evaporation of pulsed-laser illumination¹⁹. The details of sample preparation are discussed in the supplementary information. Figures 1(d) and 1(e) display the in-situ RHEED (reflection high-energy electron diffraction) patterns along $\bar{\Gamma}$ - \bar{K} and $\bar{\Gamma}$ - \bar{M} directions, and the sharp streaks indicating the high quality of the film. XRD spectrum in Fig. 1(f) shows the (001), (002), (003), (004), and (005) diffraction peaks of Mg₃Bi₂. In-plane lattice constant deduced from the RHEED streak spacing is

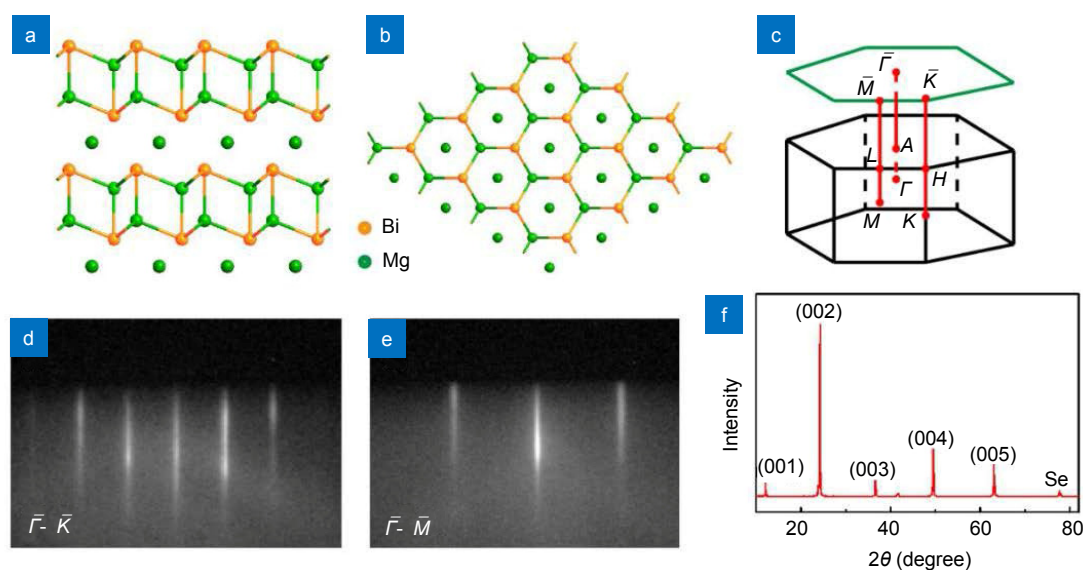


Fig. 1 | Characterization of the Mg₃Bi₂ film. Crystal structure of Mg₃Bi₂ from (a) side view and (b) top view. (c) The bulk and the projected (001) Brillouin zones of Mg₃Bi₂. RHEED patterns of the Mg₃Bi₂ film grown on the sapphire substrate, with the incident electron beam along the (d) $\bar{\Gamma}$ - \bar{K} and (e) $\bar{\Gamma}$ - \bar{M} directions, respectively. (f) XRD patterns of the Mg₃Bi₂ film, with all the (0, 0, 1n) diffraction peaks marked.

about 0.4763 nm, which is in good agreement with the results from references^{18,20}.

Terahertz emission analysis

Terahertz time-domain spectroscopy (TDS) is a crucial method to confirm the properties of topological states and the dynamics of charge carriers on a sub-picosecond timescale^{7,19,21–25}. In the process of exploring topological properties, it is significant to separate the surface signals from the bulk backgrounds^{26–28}. Fortunately, it has been verified that circularly polarized light could give rise to the asymmetric depopulation of spin-polarized surface states by optical selection rule and then generate a spin-polarized photocurrent^{6,19,26,29,30}. This transient process is known as the circular photogalvanic effect and can be detected by a femtosecond laser pulse. Based on Maxwell equations, the transient variation in the current density on picosecond timescale will generate electromagnetic radiation with the frequencies located in the THz region (1 THz = 1 ps⁻¹), which can be described by

$$E_{\text{THz}} \propto \frac{\partial J}{\partial t} \quad (1)$$

Here, E_{THz} represents the radiated electric field, and J expresses the transient current^{31,32}. The schematic view of this process can be described in Fig. 2.

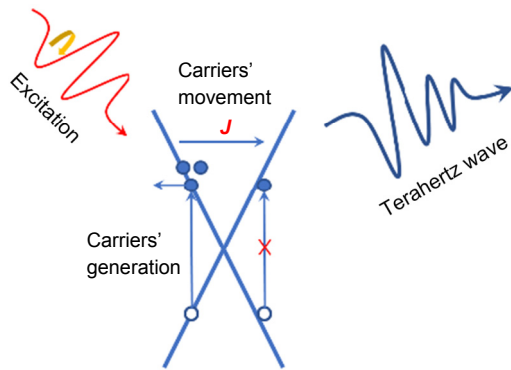


Fig. 2 | Schematic view of helicity-dependent terahertz radiation process.

In addition, THz spectroscopy is a viable contactless alternative that can complement conventional transport measurement without the necessity for electrodes or background signal that may disturb the system^{29,33}. This is especially important for the study of chiral-photocurrent in a topological system, and this technique has recently provided valuable information in topological insulators such as Bi₂Se₃^{24,30}, Sb₂Te₃¹⁹, as well as in Dirac and Weyl semimetals, like graphene^{22,34}, TaAs³⁵ and so on. Besides, the chirality-dependent photocurrents resulting from

TSSs can be controlled by the polarization of the incident light, which demonstrates the potential for optoelectronics^{19,30,36}. To date, no dynamical behavior of ultrafast photocurrent and its associated electromagnetic wave has been explored in Mg₃Bi₂, even in nodal line semimetals.

The schematic of the experimental setup is shown in Fig. 3(a) and the diagram of our terahertz emission system is depicted in Fig. S1. The Mg₃Bi₂ thin film was set up in the transmission direction of the pump light. The optical pulses with a central wavelength of 800 nm (1.55 eV) were focused on the crystal surface at an incident angle of θ to generate ultrafast photocurrent and then the terahertz wave was radiated. The vertical and horizontal components (along the E_x and E_y direction) of the emitted THz pulses were detected by electro-optical sampling, respectively. The polarization and chirality of optical pulses are controlled by rotating a quarter-wave plate (QWP) with an angle of α . The impact from bulk transient currents of Mg₃Bi₂ may contribute to the terahertz emissions in out-of-plane (perpendicular to the surface of the samples) direction, and these can be canceled by polarization settings of terahertz detection¹⁹.

The helicity-dependent terahertz emissions along the vertical direction (E_x) were measured by rotating a quarter-wave plate with an angle of α at incident angle $\theta = -45^\circ$ and $+45^\circ$, respectively, which were shown in Fig. 3. The polar plots of terahertz waveforms (0~4.5 ps) in Figs. 3(b) and 3(c) illustrate a clear polarity reversal at different helicity of optical excitations. According to the polarization trajectory, the polarization and chirality of the THz wave can be manipulated by the switching of circular or linear polarization of the incident light. Such controllability stems from the chiral ultrafast photocurrents derived from the polarized femtosecond optical pulses. Twofold symmetry was observed in the α -scan patterns, which gives more profound insights into the origins of terahertz emissions.

Figures 3(d) and 3(e) show the time domain terahertz waveforms of the Mg₃Bi₂ thin film for incident angle $\theta = -45^\circ$ and $+45^\circ$ respectively, with linearly polarized (LP, $\alpha = 0^\circ$, red line), right-hand circularly polarized (RHCP, $\alpha = 45^\circ$, black line), and left-hand circularly polarized (LHCP, $\alpha = 135^\circ$, blue line) optical excitations. The key observation is that signals obtained from the right and left-handed circularly polarized light are completely in opposite phase for both $\theta = -45^\circ$ and $+45^\circ$, and for helicity-fixed optical excitation (both RHCP and LHCP),

a similar polarity reversal was also found when the polarized light incident angle θ alternates from -45° in Fig. 3(d) to 45° in Fig. 3(e). This phenomenon usually results from the reversed incident photon helicity. THz signals from the linearly polarized light were also in the opposite phase for $\theta = -45^\circ$ and $+45^\circ$. Obviously, both the magnitude and temporal shape of the THz waveform depend strongly on the light polarization and the

incident angle. These results are consistent with the scenario for the helicity-dependent terahertz emission: the spin-polarized current generated by incident photon polarization is the major contributor to this process^{19,30-32,35}.

To further comprehend the origin of THz emission in Mg_3Bi_2 , it is essential to figure out the mechanisms behind the generation of time-resolved photocurrent. We

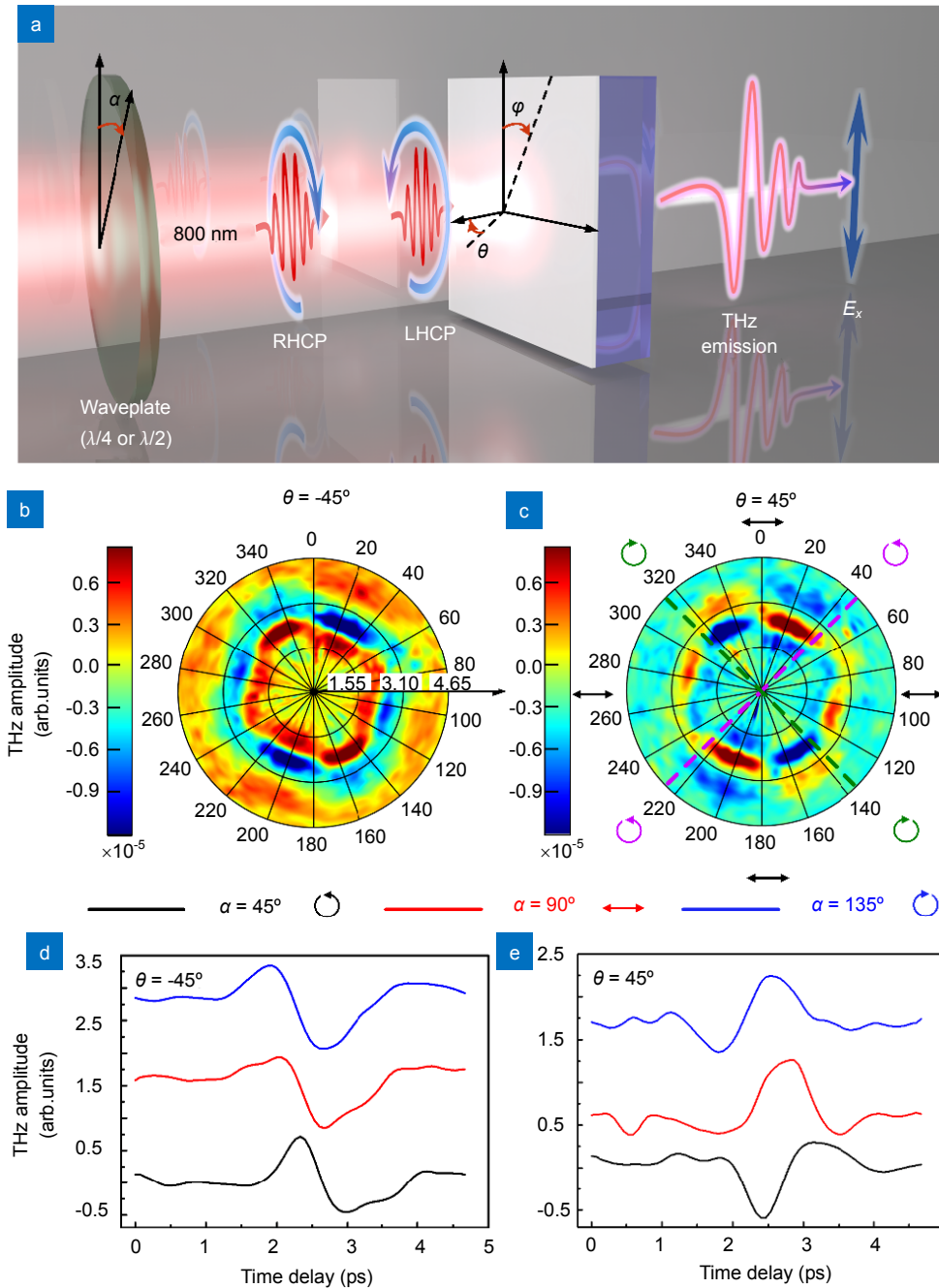


Fig. 3 | (a) Schematic of the THz emission configuration. Polar plots of terahertz waveforms (0~4.65 ps) as a function of α at (b) $\theta = -45^\circ$ and (c) $+45^\circ$, respectively, for $\varphi = 0^\circ$. The colors represent the amplitude of the terahertz emissions. Terahertz waveforms for excitation with left-hand circularly polarized, linearly polarized, and right-hand circularly polarized optical pulses at (d) $\theta = -45^\circ$ and (e) $+45^\circ$, respectively.

extracted the α -dependent THz amplitudes at the specific moment ($t = 2.46$ ps), which shows the largest variation of light response and can be controlled by rotating the QWP by an angle of α , as shown in Figs. 4(a) and 4(b). Based on the description of helicity-dependent photocurrents in topological insulators, the terahertz electric field can be inferred as $E_{\text{THz}}(\alpha, t) \propto \partial J(\alpha, t) / \partial t$ ^{7,19,30,35}. Thus, the α -dependent peak values can be well fitted using the equation as follows:

$$E_{\text{THz}(\alpha)} = C \sin(2\alpha) + L_1 \sin(4\alpha) + L_2 \cos(4\alpha) + D. \quad (2)$$

In this equation, the coefficient C represents the contribution from helicity-dependent circular photogalvanic effect. L_1 describes the helicity-independent linear photogalvanic effect^{7,19,30,35}. It has been reported that both C and L_1 are related to the topological surface states, and they are predicted to be associated with the Berry phase in spin-orbital coupled quantum well structures theoretically^{5,37}. It is worth noting that the LPGE depends on the crystal symmetry or the linear polarization of light and is generally only excited on the surface of the sample. L_2 represents the

photon drag effect (PDE), which is linked by the linear momentum transfer between incident photons and electrons. Optical rectification (OR), as a second-order nonlinear optical process, is the major process to coefficient D , which is following the well-known second-harmonic generation in noncentrosymmetric materials^{7,19,30,35,38,39}.

Based on our results, the amplitude and phase of E_x are dominated by C (CPGE, 34.87%) and L_1 (LPGE, 51.72%), which were revealed in Figs. 4(c), 4(d) and Fig. S2. The extracted CPGE component of the emitted THz electric field follows a sinusoidal dependence of 2α whose periodicity matches a change for the spin direction of the incident light. However, the LPGE part shows a 4α periodicity because it has no response to the helicity of the incident ray. Both of them are coincident with the rotational symmetry of the Dirac cone of TIs³⁷. Another $\sim 11.46\%$ component is from the polarization independent optical rectification effect, while PDE can be omitted (only 1.95%). The above results indicate that the THz emission is generated by the topological surface

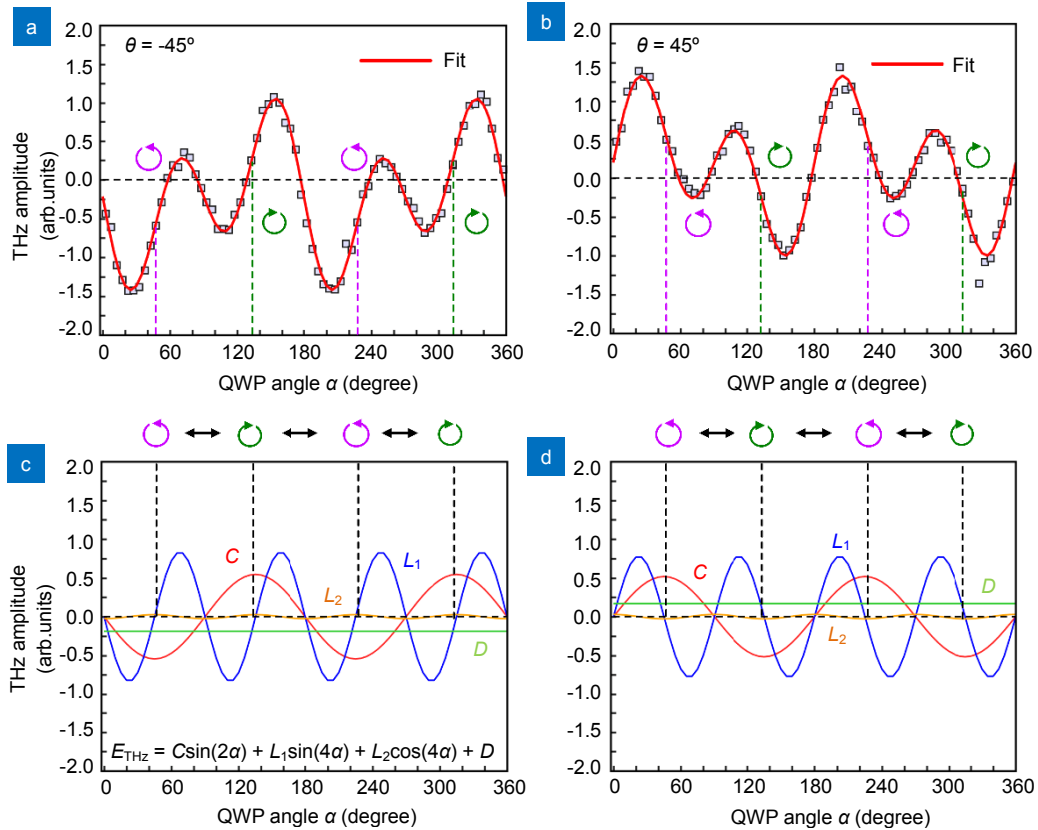


Fig. 4 | (a) and (b) represent the α -dependent terahertz amplitude at $t = 2.46$ ps. The red solid lines are the best fit with Eq. (2). The symbol \leftrightarrow , the counterclockwise arrow \odot , and the clockwise arrow \otimes denote linearly polarized (black: $\alpha = 0^\circ$), left-hand circularly polarized (pink: $\alpha = 45^\circ$), and right-hand circularly polarized (green: $\alpha = 135^\circ$) incident photons, respectively. (c) and (d) display the α -dependent coefficients C (red line), L_1 (blue line), L_2 (orange line), and D (blue line) extracted [using Eq. (2)] individually from (a) and (b).

states of the Mg_3Bi_2 thin film.

Terahertz signals in the E_y direction appear in a polarization-independent manner, which are substantially different from E_x , as shown in Fig. S3. On the one hand, signals in E_y direction are relatively weak compared with that in E_x direction. On the other hand, according to the fitting result, E_y is dominated by a polarization-independent D . L_2 plays a minor role, while C and L_1 can be neglected. These results suggest that the helicity-controlled terahertz emission mainly results from the polarization-dependent photocurrent in E_x direction, rather than the polarization-independent photocurrent in E_y direction. Such distinct features in E_x and E_y directions may lead to an elliptically polarized transient THz field⁷.

As another controllable measurement, we explore the relationship between the THz emission response and the power of incident optical pulses centered at 800 nm, with the polarization state fixed to right-hand circular polarization. It is apparent that the increase of the laser power augments the amplitude of the emitted THz waves but does not change the shape of the waveform, as shown in Fig. 5(a). Through fast Fourier transformations (FFT) of the THz waveforms, Figure 5(b) displays the frequency

domain that covers the frequency range up to 2 THz. On the other hand, the peak value for all of the spectra is centered around 0.55 THz, which is in very good agreement with the results for the time-domain analysis. Additionally, as illustrated in Fig. 5(c), a linear behavior is indicated in the dependence of the THz peak amplitude on the incident pump power up to 1800 $\mu\text{J}/\text{cm}^2$. Figure 5(d) displays the azimuthal-scan (φ -scan) results for the peak-to-peak amplitudes of the terahertz radiations with linearly polarized optical pulses at nearly normal incidence ($\theta \sim 0^\circ$) from Mg_3Bi_2 thin films. The azimuthal scan strongly depends on the crystal structure of samples. Obviously, Mg_3Bi_2 owns a centrosymmetric lattice structure for bulk, but the inversion symmetry of the top and bottom surface is broken. We deduce that the anisotropy of the azimuthal-scan results is related to the broken inversion symmetry of the surface.

To shed more light on the emission mechanism, terahertz radiation arising from the linearly polarized light can be further investigated. A half-wave plate is used to clarify the relationship between E_{THz} with the linear polarization angle α . The incident angle θ is fixed at 45° . The relationship between pump polarization angle and

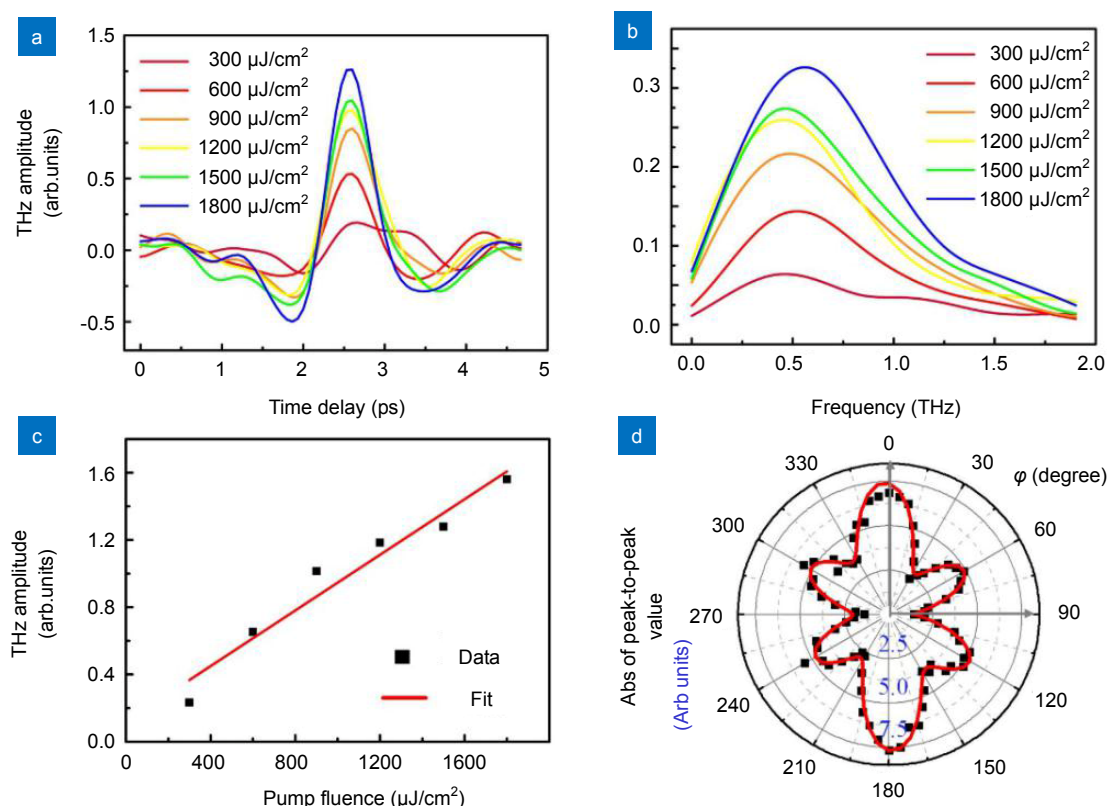


Fig. 5 | (a) THz waveforms at different photoexcitation power with the wavelength center in 800 nm. (b) Fast Fourier transformations (FFT) spectra for the directly measured terahertz waveforms that are shown in (a). (c) THz amplitude versus the power of the incident laser beam. (d) The azimuthal dependent (φ -dependent) absolute amplitude of THz emission waveforms with linear polarized optical pulses.

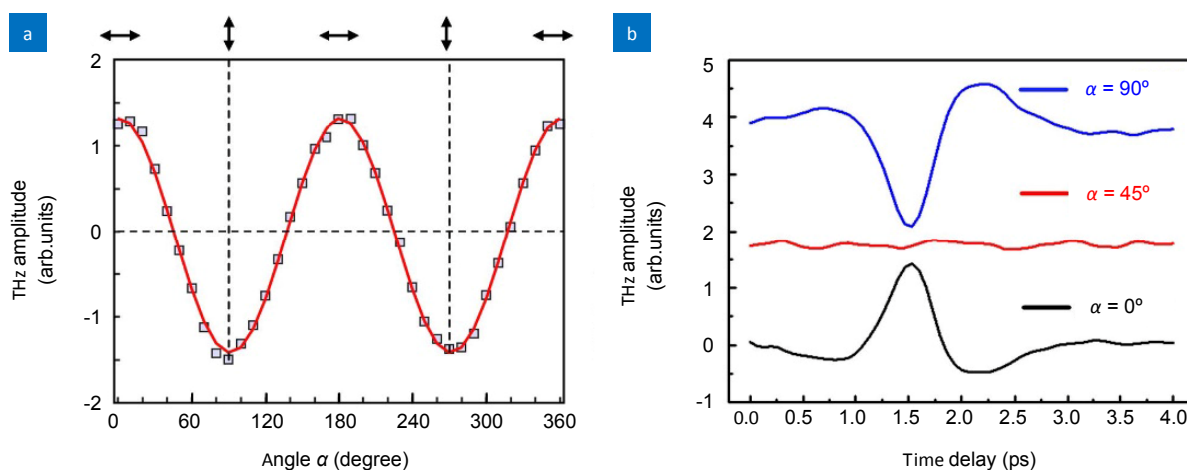


Fig. 6 | (a) THz amplitude as a function of the linear polarization angle α . The red solid line shows the fitting results using a sinusoidal function. (b) Terahertz waveforms for excitation with a linearly polarized angle at $\alpha = 0^\circ$, 45° and 90° , respectively.

terahertz amplitude near the peak values is shown in Fig. 6(a). We found that E_{THz} induced by the linearly polarized light can be well described by a sinusoidal function with a period of 180° . The amplitude of the wave excited by linearly polarized light is approximately three times smaller than that of the wave excited by circularly polarized light, compared with Figs. 4(a) and 4(b). When the polarization angle of the pump beam α is changed from 0° to 90° , the polarity of the emitted THz pulse is reversed, as shown in Fig. 6(b). No THz emission is detected at a polarization angle of $\alpha = 45^\circ$. This phenomenon can be described by a second-order nonlinear optical process⁷. The different intensity and period of terahertz signals excited by linearly or circularly polarized light further verified the dominant role of topological surface states in spintronic terahertz emission.

Summary and discussions

In conclusion, for the first time, we demonstrated that spin photocurrent induced helicity-dependent terahertz emission could be realized in nodal-line semimetal candidate Mg_3Bi_2 . The polarization directions and magnitudes of helical THz wave can be easily controlled without any THz waveplate. The polarization control is mainly originated from polarity-dependent photocurrent, and then can be effectively manipulated by circular photogalvanic effect. Such an intrinsic spintronic emitter shows promising characteristics and is easily accessible. Finally, this work will open up intriguing opportunities for fundamental studies of novel THz emission, THz spintronics, and THz modulation devices by using topological materials⁴⁰.

References

- Lodahl P, Mahmoodian S, Stobbe S, Rauschenbeutel A, Schneeweiss P et al. Chiral quantum optics. *Nature* **541**, 473–480 (2017).
- Kampfrath T, Sell A, Klatt G, Pashkin A, Mährlein S et al. Coherent terahertz control of antiferromagnetic spin waves. *Nat Photonics* **5**, 31–34 (2011).
- Wolf S A, Awschalom D D, Buhrman R A, Daughton J M, von Molnár S et al. Spintronics: a spin-based electronics vision for the future. *Science* **294**, 1488–1495 (2001).
- Ferguson B, Zhang X C. Materials for terahertz science and technology. *Nat Mater* **1**, 26–33 (2002).
- McIver J W, Hsieh D, Steinberg H, Jarillo-Herrero P, Gedik N. Control over topological insulator photocurrents with light polarization. *Nat Nanotechnol* **7**, 96–100 (2012).
- Braun L, Mussler G, Hruban A, Konczykowski M, Schumann T et al. Ultrafast photocurrents at the surface of the three-dimensional topological insulator Bi_2Se_3 . *Nat Commun* **7**, 13259 (2016).
- Gao Y, Kaushik S, Philip E J, Li Z, Qin Y et al. Chiral terahertz wave emission from the Weyl semimetal TaAs. *Nat Commun* **11**, 720 (2020).
- Zhang Z L, Chen Y P, Cui S, He F, Chen M et al. Manipulation of polarizations for broadband terahertz waves emitted from laser plasma filaments. *Nat Photonics* **12**, 554–559 (2018).
- Burkov A A, Hook M D, Balents L. Topological nodal semimetals. *Phys Rev B* **84**, 235126 (2011).
- Fang C, Chen Y G, Kee H Y, Fu L. Topological nodal line semimetals with and without spin-orbital coupling. *Phys Rev B* **92**, 081201 (2015).
- Bian G, Chang T R, Sankar R, Xu S Y, Zheng H et al. Topological nodal-line fermions in spin-orbit metal PbTaSe_2 . *Nat Commun* **7**, 10556 (2016).
- Bian G, Chang T R, Zheng H, Velury S, Xu S Y et al. Drumhead surface states and topological nodal-line fermions in TlTaSe_2 . *Phys Rev B* **93**, 121113 (2016).
- Yang S Y, Yang H, Derunova E, Parkin S S P, Yan B H et al. Symmetry demanded topological nodal-line materials. *Adv Phys: X* **3**, 1414631 (2018).
- Yu R, Weng H M, Fang Z, Dai X, Hu X. Topological node-line

- semimetal and dirac semimetal state in antiperovskite Cu_3PdN . *Phys Rev Lett* **115**, 036807 (2015).
15. Wu Y, Wang L L, Mun E, Johnson D D, Mou D X et al. Dirac node arcs in PtSn_4 . *Nat Phys* **12**, 667–671 (2016).
 16. Chang T R, Pletikoscic I, Kong T, Bian G, Huang A et al. Realization of a type-II nodal-line semimetal in Mg_3Bi_2 . *Adv Sci* **6**, 1800897 (2019).
 17. Mao J, Zhu H T, Ding Z W, Liu Z H, Gamage G A et al. High thermoelectric cooling performance of n-type Mg_3Bi_2 -based materials. *Science* **365**, 495–498 (2019).
 18. Zhou T, Zhu X G, Tong M Y, Zhang Y, Luo X B et al. Experimental evidence of topological surface states in Mg_3Bi_2 films grown by molecular beam epitaxy. *Chin Phys Lett* **36**, 117303 (2019).
 19. Tu C M, Chen Y C, Huang P, Chuang P Y, Lin M Y et al. Helicity-dependent terahertz emission spectroscopy of topological insulator Sb_2Te_3 thin films. *Phys Rev B* **96**, 195407 (2017).
 20. Zhang X M, Jin L, Dai X F, Liu G D. Topological Type-II nodal line semimetal and dirac semimetal state in stable kagome compound Mg_3Bi_2 . *J Phys Chem Lett* **8**, 4814–4819 (2017).
 21. Sánchez-Barriga J, Golias E, Varykhalov A, Braun J, Yashina L V et al. Ultrafast spin-polarization control of Dirac fermions in topological insulators. *Phys Rev B* **93**, 155426 (2016).
 22. Maysonave J, Huppert S, Wang F, Maero S, Berger C et al. Terahertz generation by dynamical photon drag effect in graphene excited by femtosecond optical pulses. *Nano Lett* **14**, 5797–5802 (2014).
 23. Plank H, Golub L E, Bauer S, Bel'kov V V, Herrmann T et al. Photon drag effect in $(\text{Bi}_{1-x}\text{Sb}_x)_2\text{Te}_3$ three-dimensional topological insulators. *Phys Rev B* **93**, 125434 (2016).
 24. Zhu L G, Kubera B, Fai Mak K, Shan J. Effect of surface states on terahertz emission from the Bi_2Se_3 surface. *Sci Rep* **5**, 10308 (2015).
 25. Zhang K X, Zhang Y Z, Wang X C, Yan T M, Jiang Y H. Continuum electron giving birth to terahertz emission. *Photonics Res* **8**, 760–767 (2020).
 26. Bas D A, Muniz R A, Babakiray S, Lederman D, Sipe J E et al. Photocurrents in Bi_2Se_3 : bulk versus surface, and injection versus shift currents. *Opt Express* **24**, 23583 (2016).
 27. Park B C, Kim T H, Sim K I, Kang B Y, Kim J W et al. Terahertz single conductance quantum and topological phase transitions in topological insulator Bi_2Se_3 ultrathin films. *Nat Commun* **6**, 6552 (2015).
 28. He L, Xiu F X, Yu X X, Teague M, Jiang W J et al. Surface-dominated conduction in a 6 nm thick Bi_2Se_3 thin film. *Nano Lett* **12**, 1486–1490 (2012).
 29. Pan Y, Wang Q Z, Yeats A L, Pillsbury T, Flanagan T C et al. Helicity dependent photocurrent in electrically gated $(\text{Bi}_{1-x}\text{Sb}_x)_2\text{Te}_3$ thin films. *Nat Commun* **8**, 1037 (2017).
 30. Hamh S Y, Park S H, Jerng S K, Jeon J H, Chun S H et al. Helicity-dependent photocurrent in a Bi_2Se_3 thin film probed by terahertz emission spectroscopy. *Phys Rev B* **94**, 161405 (2016).
 31. Kampfrath T, Battiato M, Maldonado P, Eilers G, Nötzold J et al. Terahertz spin current pulses controlled by magnetic heterostructures. *Nat Nanotechnol* **8**, 256–260 (2013).
 32. Kinoshita Y, Kida N, Miyamoto T, Kanou M, Sasagawa T et al. Terahertz radiation by subpicosecond spin-polarized photocurrent originating from Dirac electrons in a Rashba-type polar semiconductor. *Phys Rev B* **97**, 161104 (2018).
 33. Wu Y, Elyasi M, Qiu X P, Chen M J, Liu Y et al. High-performance THz emitters based on ferromagnetic/nonmagnetic heterostructures. *Adv Mater* **29**, 1603031 (2017).
 34. Bahk Y M, Ramakrishnan G, Choi J, Song H, Choi G et al. Plasmon enhanced terahertz emission from single layer graphene. *ACS Nano* **8**, 9089–9096 (2014).
 35. Sirica N, Tobey R I, Zhao L X, Chen G F, Xu B et al. Tracking ultrafast photocurrents in the Weyl semimetal TaAs using THz emission spectroscopy. *Phys Rev Lett* **122**, 197401 (2019).
 36. Chen M J, Wu Y, Liu Y, Lee K, Qiu X P et al. Current - enhanced broadband THz emission from spintronic devices. *Adv Opt Mater* **7**, 1801608 (2019).
 37. Moore J E, Orenstein J. Confinement-induced berry phase and helicity-dependent photocurrents. *Phys Rev Lett* **105**, 026805 (2010).
 38. Dong J P, Gradwohl K P, Xu Y D, Wang T, Zhang B B et al. Terahertz emission from layered GaTe crystal due to surface lattice reorganization and in-plane noncubic mobility anisotropy. *Photonics Res* **7**, 518–525 (2019).
 39. Miltos Maragkakis G, Psilodimitrakopoulos S, Mouchliadis L, Paradisanos I, Lemonis A et al. Imaging the crystal orientation of 2D transition metal dichalcogenides using polarization-resolved second-harmonic generation. *Opto-Electron Adv* **2**, 190026 (2019).
 40. Hu Y Z, Jiang T, Zhou J H, Hao H, Sun H et al. Ultrafast terahertz frequency and phase tuning by all-optical molecularization of metasurfaces. *Adv Optical Mater* **7**, 1901050 (2019).

Acknowledgements

We thank Prof. J. B. Qi for helpful discussions and are grateful for financial support from the National Natural Science Foundation of China (Grant Nos.11804387, 11802339, 11805276, 11902358, 61805282, and 61801498); the Scientific Researches Foundation of National University of Defense Technology (Grant Nos. ZK18-03-22, ZK18-01-03 and ZK18-03-36).

Author contributions

M. Y. Tong and Y. Z. Hu contributed equally to this work. J. Tian and M. Y. Tong conceived the idea and designed the research; M. Y. Tong and X. N. Xie fabricated all the samples; Y. Z. Hu performed the optical measurement. T. Jiang, Z. Y. Wang, X. A. Cheng and X. G. Zhu analysed the data; M. Y. Tong and Y. Z. Hu co-wrote the manuscript. All authors discussed and commented on the manuscript.

Competing interests

The authors declare no competing financial interests.

Supplementary information

Supplementary information for this paper is available at <https://doi.org/10.29026/oea.2020.200023>